SLAC-PUB-1495
October 1974
(T/E)

CHARGED HADRON MULTIPLICITIES AND TOPOLOGIES IN INELASTIC μ^-p SCATTERING*

J. Ballam, E. D. Bloom, J. T. Carroll, G. B. Chadwick, R. L. A. Cottrell, M. Della Negra,† H. DeStaebler, L. K. Gershwin,‡ L. P. Keller, M. D. Mestayer, K. C. Moffeit, C. Y. Prescott, S. Stein

Stanford Linear Accelerator Center
Stanford University, Stanford, California 94305

ABSTRACT

We report the final state charged-hadron multiplicities and topological cross sections for inelastic scattering of 16 GeV μ^-'s from hydrogen in the SLAC 40-inch bubble chamber. We find that for $1.8 \leq W \leq 5.0$ GeV the charged hadron multiplicity is generally lower at $Q^2 = 1.5$ GeV^2 than for photoproduction.

(Submitted to Phys. Rev. Letters)

---

* Work supported by the U.S. Atomic Energy Commission.

† Present address: College de France, Paris, France.

‡ Present address: Institute for Defense Analysis, Washington, D. C.

In this letter we present some results of a hybrid bubble chamber experiment examining the process

$$\mu^- + p \rightarrow \mu^- + X^+(W)$$

where the charged tracks in the final state X^+, which has mass W, are detected with 4π geometry. A study of the properties of the hadronic final state was undertaken to provide further experimental information on the nature of scaling phenomena observed in the SLAC-MIT inelastic electron scattering experiments. Here we concentrate on one aspect of the hadronic final state, the charged particle multiplicity. This and the associated topological cross sections, including those for visible strange particles, will be discussed here. A more complete description of the experiment, kinematics, and additional but preliminary results, was presented earlier.[1] For a discussion of vector meson production in this experiment see Ref. 2.

This experiment was performed at SLAC using a secondary 16 GeV/c μ^- beam into the 40-inch hydrogen bubble chamber. The chamber flash lamps were triggered by a μ telescope placed downstream from the bubble chamber. This telescope consisted of two scintillation counter hodoscopes and 11 magnetostrictive wire spark chambers sandwiched between four 1-ft. thick pieces of steel. When an online trigger indicated a μ-scatter of $\gtrsim 1.4^{\circ}$, a picture was taken, and spark chamber and counter information were recorded on magnetic tape. Reconstructed events occurring in the bubble chamber fiducial volume were required to have a negative track coincide with penetrating spark chamber tracks. This procedure yielded 3723 inelastic and 1043 elastic events, representing 5000 events per microbarn. During the majority of the data taking time, the bubble chamber pulsed at 10 expansions per second, with an average of 100 μ's per pulse.

Particular care was taken to eliminate π's from the trigger. Beryllium placed in the beam transport system reduced the incident π's to a measured value of $\pi/\mu = (5 \pm 2) \times 10^{-5}$. The 12 interaction lengths of iron in the telescope suppressed triggers from final state π's. The π-induced contamination in the final data sample was measured to be less than 1%.

In the reconstruction process the outgoing μ^- was separated from all tracks emerging from the vertex in the bubble chamber by using the recorded μ^- telescope information. Combining the telescope information with that in the bubble chamber also improved the momentum measurement of the μ^- by a factor of 15, on the average. In Figure 1 we show the distribution of the 4766 events in a scatter plot of Q^2 vs W. Elastic events can be seen clearly as a vertical line at the proton mass. Inelastic events extend to about $Q^2 = 3.0$ GeV^2 and W = 5.0 GeV. Superimposed on the scatter plot are contours of the detection probability, P, for scattered muons in this experiment as obtained from a Monte Carlo calculation. The charged hadron multiplicities and partial topological cross section ratios are insensitive to P.

The flux of muons in our beam was monitored with scintillation counters in the beam. This enabled us to extract the observed cross section and compare it to known ep inclusive cross sections. In the determination of σ (up) we have made small corrections for scanning inefficiency (1%), spark chamber inefficiency (3%), unmeasurable events (2%), pion contamination (1%), and radiative corrections (typically 5%). We estimate a 12% average systematic error in the absolute cross section based on uncertainties in P (±10%), absolute beam flux (±5%), spark chamber efficiencies (±3%), and scanning and measurement losses (±2%). Combining all our inelastic data, we obtain

$$\sigma(\mu p)/\sigma(ep) = 0.91 \pm 0.12.$$

The error is a combination of statistical (2%) and estimated systematic errors (12% for this experiment and 5% for ep cross sections).[3]

Next we consider relative prong cross sections, σ_n/σ_{tot}, where n is the number of charged hadron prongs in the final state. Table I gives σ_n/σ_{tot} for n = 1, 3, 5, and 7 (only four events were found with an apparent even prong number). Also given are relative partial cross section ratios for strange particle production with visible decays, σ_{st}/σ_{tot}. For comparison these same quantities are given for photoproduction.[4] In Figure 2a and Table I we show the relative contribution of each topology to the cross section for increasing Q^2 in three W ranges. No strong Q^2 dependence is seen, within errors, for n = 5 or 7 prongs or strange topologies. However, as seen in Figure 2a, σ_1/σ_{tot} tends to increase as Q^2 increases, while for the lowest W bin σ_3/σ_{tot} tends to decrease.

We now compute the mean charged hadron multiplicity $\langle N \rangle$.

$$\langle N \rangle = \frac{\sum_{\text{events}} n_i/P_i}{\sum_{\text{events}} 1/P_i} = \frac{\sum_{\text{prongs}} n\sigma_n}{\sum_{\text{prongs}} \sigma_n}$$

where n_i is the number of prongs in the ith event, P_i is the muon detection probability mentioned previously and σ_n is the partial cross section for n-prong events. We have applied radiative corrections to the data.[5]

In Figure 2b, $\langle N \rangle$ is plotted as a function of Q^2 for fixed W ranges.[7] Also shown are the photoproduction values at $Q^2 = 0$, obtained from the data of Ref. 4. We observe that for the two lower W intervals $\langle N \rangle$ decreases by 10% to 15% below the photoproduction values. For the high W bin, a flat Q^2 dependence cannot be ruled out.

These trends cannot be explained solely by the behavior of the vector

meson cross sections.[2,6] When one attempts to remove the ρ contribution using a model of ρ photoproduction and ρ electroproduction,[2] one finds less than a 3% change in $\langle N \rangle$ in any of the data points, and a relative change in a single $\langle W \rangle$ bin of less than 2%.

Figure 3 shows the mean charged multiplicity plotted versus W^2. Here data from two electroproduction experiments[8,9] and from photoproduction[4] are also included. Fitting our data for $Q^2 \geq .24$ to a logarithmic dependence in W^2, we obtain

$$\langle N \rangle = (.89 \pm .14) + (.92 \pm .07) \ln W^2$$

which falls below the photoproduction line but approximately parallel to it. These results are in good agreement with those of Ref. 8 but appear to disagree with Ref. 9.

In conclusion, we find that for $1.8 \leq W \leq 5.0$ GeV, $\langle N \rangle$ generally decreases as Q^2 increases at fixed W, and that this is primarily due to an increase in $\sigma_1/\sigma(\mu p)$ and a decrease in $\sigma_3/\sigma(\mu p)$.

We wish to thank Bob Watt and the crew of the 40-inch bubble chamber for 30 million good expansions.

REFERENCES

1. J. Ballam et al., Stanford Linear Accelerator Center Report No. SLAC-PUB-1143 (1973); and E.D. Bloom, XVI International Conference on High Energy Physics, Batavia, Ill., September 6-13, 1972 (National Accelerator Laboratory, Batavia, Ill., 1973); Vol. 2, p. 66.

2. J. Ballam et al., Stanford Linear Accelerator Center Report No. SLAC-PUB-1373 (1974), to be published in Phys. Rev. D (August 1974).

3. G. Miller et al., Phys. Rev. D 5, 528 (1972). For the inelastic cross

section we used a phenomenological fit to the MIT-SLAC electroproduction data developed by W. Atwood and S. Stein (private communication).

4. SLAC-LBL-Tufts collaboration, J. Ballam et al., Phys. Rev. D 5, 545 (1972), and H. H. Bingham et al., Phys. Rev. D 8, 1277 (1973). The values of $\langle N \rangle_\gamma$ at the mean values of W obtained in our experiment were interpolated in $\ell n W^2$ between the data points of this reference.

5. The radiative corrections were performed using the radiative formulae presented in Ref. 3. These formulae were modified for muons, and the needed elastic and inelastic cross sections were derived from fits described in Ref. 3. The elastic correction, which involves 1-prongs only, was never more than 10%. The inelastic correction, based on a model using $\langle N \rangle = 1.08 + 0.91\, \ell n\, W^2$ independent of Q^2, was never more than 5%.

6. J.T. Dakin et al., Phys. Rev. Letters 30, 142 (1973); and V. Eckardt et al., Nucl. Phys. B55, 45 (1973).

7. The values of $\langle N \rangle$ are corrected to the same $\langle W \rangle$ using $\langle N \rangle = 1.08 + 0.910\, \ell n\, W^2$ independent of Q^2. The corrections thus obtained are never greater than 0.5 standard deviation and usually are much less.

8. V. Eckardt et al., DESY Report DESY 74/5 (February 1974).

9. P.H. Garbincius et al., Phys. Rev. Letters 32, 328 (1974).

TABLE CAPTION

I. Partial cross section ratios for n = 1, 3, 5, and 7 prong events. Strange particles are included in the prong distributions. Visible strange particle production is also shown separately. σ_1 has been corrected for elastic radiative effects. The mean charged hadron multiplicities $\langle N \rangle$ are radiatively corrected values and are adjusted to the $\langle W \rangle$ values shown for the photoproduction points.

TABLE I

<W> (GeV)	Q^2 (GeV^2)	NUMBER	σ_1/σ_{tot}	σ_3/σ_{tot}	σ_5/σ_{tot}	σ_7/σ_{tot}	σ_{st}/σ_{tot}	< N >
				Inelastic μp				
2.24	.25	382	.31 ± .03	.64 ± .04	.04 ± .01	-	.06 ± .01	2.49 ± .06
2.27	.56	290	.35 ± .04	.63 ± .05	.02 ± .01	-	.06 ± .02	2.36 ± .06
2.27	.95	137	.42 ± .06	.53 ± .06	.04 ± .02	-	.07 ± .02	2.25 ± .10
2.25	1.74	106	.42 ± .06	.54 ± .07	.03 ± .02	-	.04 ± .02	2.24 ± .11
3.25	.24	269	.18 ± .03	.59 ± .05	.21 ± .03	.014± .008	.06 ± .01	3.18 ± .09
3.16	.54	155	.22 ± .04	.61 ± .06	.17 ± .03	.006± .006	.09 ± .03	3.02 ± .11
3.24	.95	78	.17 ± .05	.63 ± .09	.18 ± .05	.026± .019	.11 ± .05	3.18 ± .16
3.28	1.80	67	.22 ± .06	.68 ± .10	.09 ± .04	.012± .012	.06 ± .03	2.80 ± .14
4.30	.0675	335	.00 ± .06	.67 ± .05	.29 ± .04	.05 ± .01	.10 ± .02	3.76 + .12
4.24	.25	186	.14 ± .05	.57 ± .06	.27 ± .04	.05 ± .02	.10 ± .02	3.49 ± .13
4.33	.56	80	.14 ± .06	.46 ± .08	.31 ± .07	.08 ± .03	.08 ± .03	3.61 ± .21
4.27	1.38	39	.20 ± .09	.46 ± .12	.31 ± .10	.02 ± .02	.07 ± .03	3.37 ± .38
				Photoproduction				
2.25	.00		.24 ± .02	.73 ± .02	.03 ± .01	-	.055± .01	2.53 ± .04
3.25	.00		.12 ± .02	.68 ± .02	.19 ± .02	.01 ± .003	.069± .01	3.13 ± .03
4.25	.00		.07 ± .01	.56 ± .02	.30 ± .02	.06 ± .01	.075± .004	3.66 ± .03

FIGURE CAPTIONS

1. Scatter plot of Q^2(GeV^2) vs W(GeV) for 4766 events. Superimposed on the data are contours of P, the outgoing μ detection probability.

2a. The fractional part of σ_{tot} contributed by n = 1, 3, 5, and 7 prong events vs Q^2 for three ranges of W. The open symbols show photoproduction data.

2b. The mean charged hadron multiplicity vs Q^2 for three ranges of W.

3. The mean charged hadron multiplicity vs W^2.

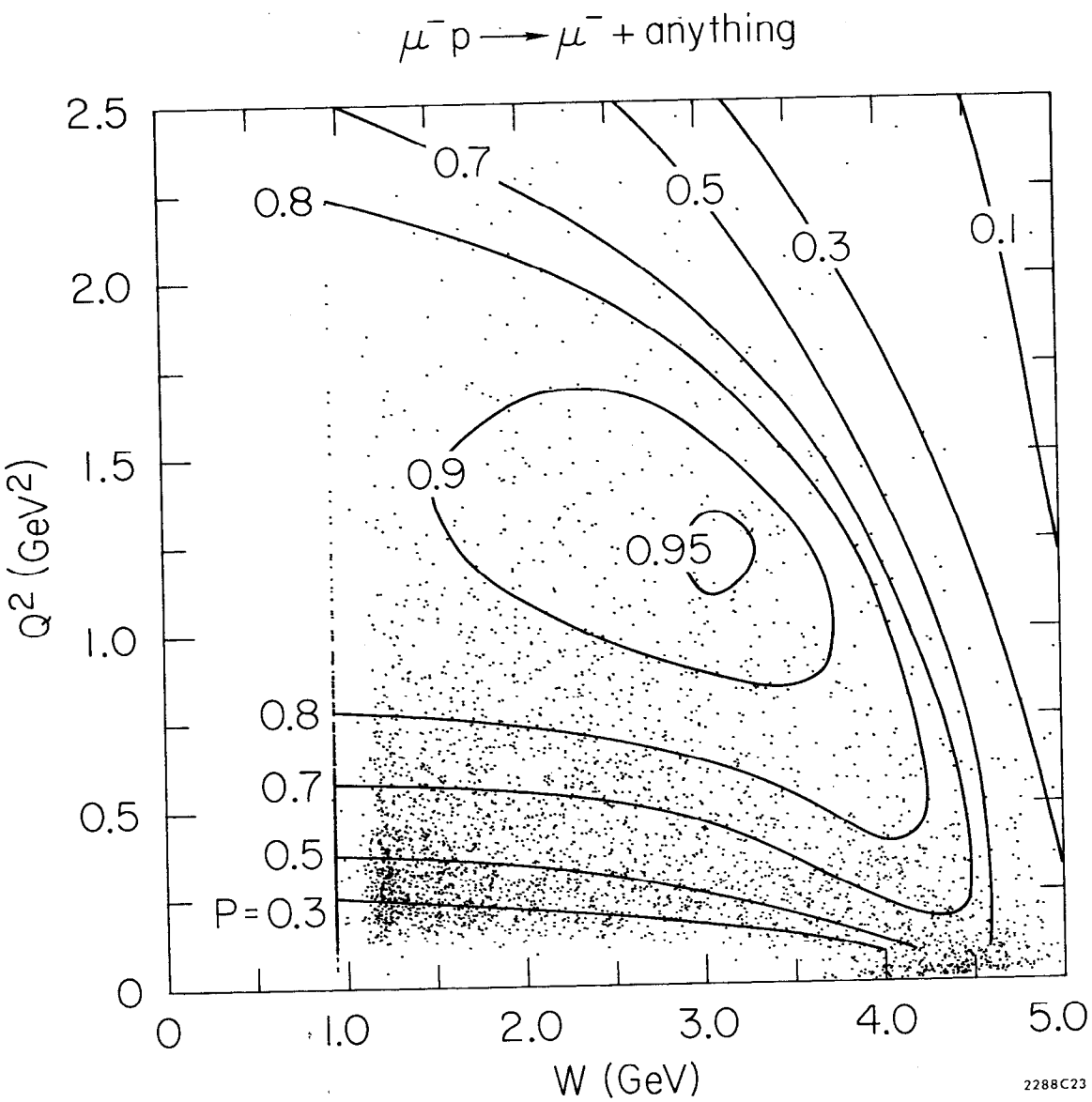
$\mu^- p \longrightarrow \mu^-$ + anything
2.5
2.0
1.5
1.0
0.5
0
Q^2 (GeV^2)
0.7
0.8
0.5
0.3
0.1
0.9
0.95
0.8
0.7
0.5
P = 0.3
0
1.0
2.0
3.0
4.0
5.0
W (GeV)
2288C23

Fig. 1

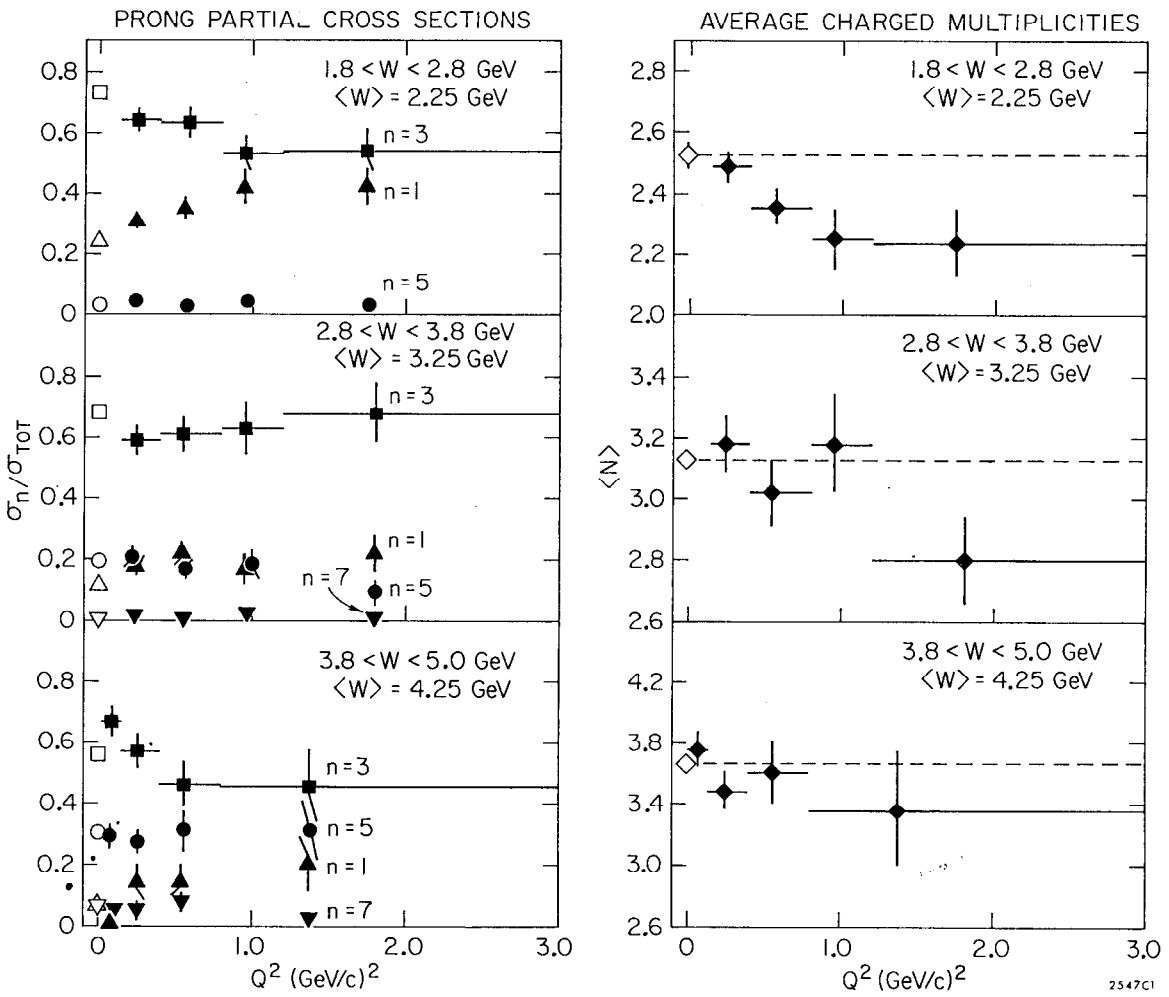
PRONG PARTIAL CROSS SECTIONS
AVERAGE CHARGED MULTIPLICITIES
1.8 < W < 2.8 GeV
⟨W⟩ = 2.25 GeV
2.8 < W < 3.8 GeV
⟨W⟩ = 3.25 GeV
3.8 < W < 5.0 GeV
⟨W⟩ = 4.25 GeV
n = 1
n = 3
n = 5
n = 7
σn/σTOT
⟨N⟩
Q2 (GeV/c)2
2547C1

Fig. 2

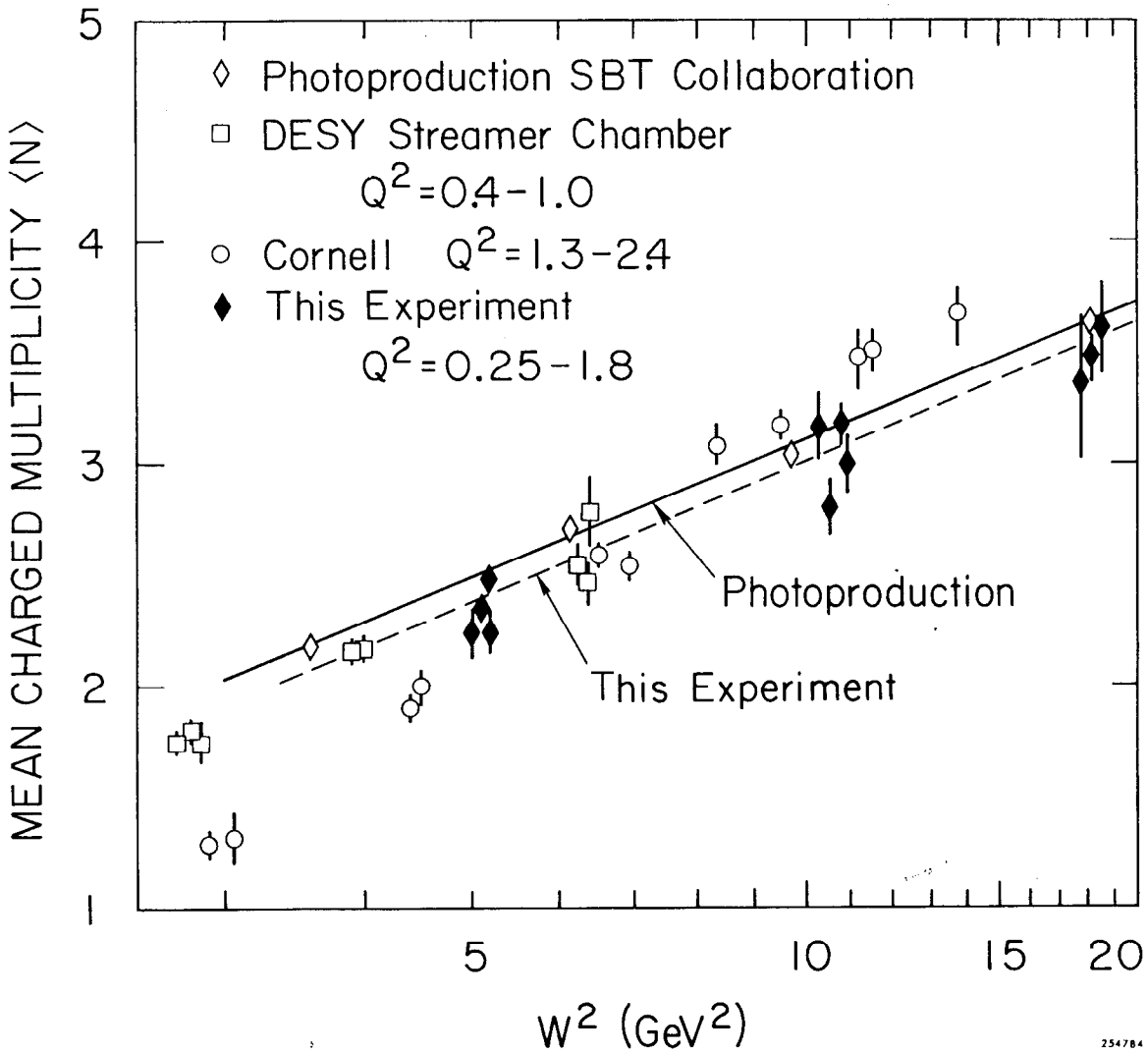
Photoproduction SBT Collaboration
DESY Streamer Chamber
Q^2=0.4-1.0
Cornell Q^2=1.3-2.4
This Experiment
Q^2=0.25-1.8
Photoproduction
This Experiment
MEAN CHARGED MULTIPLICITY ⟨N⟩
W^2 (GeV^2)
1
2
3
4
5
5
10
15
20
2547B4

Fig. 3